sponse. A perfectly reflecting, white Lambertian disk would have an *I/F* of 1.0.
7. P. M. Beauchamp *et al.*, in *Proceedings of the 8th Annual AIAA/ Utah State University Conference on Small Satellites*, Logan, UT, 29 August to 1 September 1994.
8. L. A. Soderblom *et al.*, in *Proceedings of the DS1 Technology Validation Symposium*, Pasadena, CA, 8 to 9 February 2000.
9. *IAU Minor Planet Circular 31664* (1998).
10. Comet 19P/Borrelly was discovered on 28 December 1904 by Alphonse Louis Nicolas Borrelly of Marseilles, France.
11. P. L. Lamy *et al.*, *Astron. Astrophys.* **337**, 945 (1998).
12. P. Farinella, D. R. Davis, S. A. Stern, in *Protostars and Planets IV*, V. Mannings, A. P. Boss, S. S. Russell, Eds. (Univ. of Arizona Press, Tucson, AZ, 2000), p. 1255.
13. P. R. Weissman, *Nature* **320**, 242 (1986).
14. H. Rauer *et al.*, *Bull. Am. Astron. Soc.* **31**, 1131 (1999).
15. J. Veverka *et al.*, *Science* **278**, 2109 (1997).
16. B. Clark *et al.*, *Icarus* **140**, 53 (1999).
17. M. S. Hanner *et al.*, *Icarus* **62**, 97 (1985).
18. G. J. Veeder *et al.*, *Astron. J.* **94**, 169 (1987).
19. E. Tedesco *et al.*, *Astron. J.* **97**, 580 (1989).
20. M. E. Ockert *et al.*, *J. Geophys. Res.* **92**, 14969 (1987).
21. B. J. Buratti, J. A. Mosher, *Icarus* **115**, 219 (1995).
22. W. F. Huebner, *Science* **237**, 628 (1987).
23. D. L. Mitchell *et al.*, *Science* **237**, 626 (1987).
24. D. P. Cruikshank *et al.*, *Icarus* **135**, 389 (1988).
25. J. Knollenberg *et al.*, *Earth Moon Planets* **72**, 103 (1996).
26. I. Konno *et al.*, *Icarus* **116**, 77 (1995).
27. B. Mueller, N. Samarasinha, *Bull. Am. Astron. Soc.* **33**, 1090 (2001).
28. B. G. Marsden, *IAU Circular 7771* (2001).

3 January 2002; accepted 26 March 2002
Published online 4 April 2002;
10.1126/science.1069527
Include this information when citing this paper.

The *E. coli* BtuCD Structure: A Framework for ABC Transporter Architecture and Mechanism

Kaspar P. Locher,* Allen T. Lee, Douglas C. Rees*

The ABC transporters are ubiquitous membrane proteins that couple adenosine triphosphate (ATP) hydrolysis to the translocation of diverse substrates across cell membranes. Clinically relevant examples are associated with cystic fibrosis and with multidrug resistance of pathogenic bacteria and cancer cells. Here, we report the crystal structure at 3.2 angstrom resolution of the *Escherichia coli* BtuCD protein, an ABC transporter mediating vitamin B_{12} uptake. The two ATP-binding cassettes (BtuD) are in close contact with each other, as are the two membrane-spanning subunits (BtuC); this arrangement is distinct from that observed for the *E. coli* lipid flippase MsbA. The BtuC subunits provide 20 transmembrane helices grouped around a translocation pathway that is closed to the cytoplasm by a gate region whereas the dimer arrangement of the BtuD subunits resembles the ATP-bound form of the Rad50 DNA repair enzyme. A prominent cytoplasmic loop of BtuC forms the contact region with the ATP-binding cassette and appears to represent a conserved motif among the ABC transporters.

Since its discovery over a decade ago, the family of ABC transporter proteins has grown dramatically to well over a thousand examples with known sequences. ABC transporters now form the largest family of membrane-spanning transport proteins, ubiquitous in all branches of life (*1*). They invariably consist of two membrane-spanning domains that harbor a translocation pathway for a specific substrate, and two attached, water-exposed, and well-conserved ATP-binding cassettes (hence ABC) that power the transport reaction through hydrolysis of ATP (*2*, *3*). Several mammalian ABC transporters are medically relevant. For example, mutations in the cystic fibrosis transmembrane conductance regulator (CFTR) cause a dysfunction of this protein that represents the molecular basis of cystic fibrosis (*4*). A separate subclass of ABC transporters are related to multidrug resistance, exemplified by the human MDR1 and MRP1 proteins, whose overexpression in tumor cells causes resistance to various cytotoxic agents used in chemotherapy (*5*). Another clinically relevant ABC transporter is the TAP protein, which translocates antigenic polypeptides from the cytoplasm into the endoplasmic reticulum, where they are being loaded onto major histocompatibility complex (MHC) class I molecules (*6*, *7*). In bacteria, ABC transporters are predominantly involved in nutrient uptake, although they also participate in the export of bacterial toxins or harmful substances, contributing to bacterial multidrug resistance (*8*, *9*). Bacterial ABC transporters are generally assembled from up to four separate protein subunits, whereas their eukaryotic counterparts are generally composed of a single polypeptide.

A striking feature of the ABC transporter family is that it includes importers and exporters, and that the recognized substrates range from single chloride ions (in CFTR) to entire protein toxins (bacterial toxin exporters). This diversity of transported substrates is reflected in the poor sequence similarities of the membrane-spanning subunits and domains. What ties the family together are a number of highly conserved ABC cassette motifs (Fig. 1), many of which are directly involved in the binding and hydrolysis of ATP, such as the P loop or Walker-A motif, the Walker-B motif, a glutamine residue in the Q loop, and a histidine residue in the Switch region (*10*–*12*). In addition, ABC cassettes invariably possess a D loop (*13*) and a short polypeptide stretch (. . . LSGG . . .), which is so specific to this protein class that it is generally referred to as the "ABC signature sequence." In view of these similarities, it is generally assumed that all ABC cassettes bind and hydrolyze ATP in a similar fashion and use a common mechanism to power the translocation of substrate through the membrane-spanning partner domains.

The current view of the mechanism begins with binding of the substrate to the transporter. Importers in Gram-negative bacteria generally require a periplasmic binding protein that delivers the substrate to the periplasmic side of the transporter (*14*), whereas exporters recruit their substrates directly from the cytoplasm or, in the case of very hydrophobic substances, from the inner leaflet of the plasma membrane. The binding event is signaled to the nucleotide hydrolysis sites, where it is thought to increase the affinity for ATP, a prerequisite for a productive transport cycle. The two ABC cassettes then carry out the "power stroke," a highly cooperative ATP-binding and hydrolysis reaction that is concurrent with a substantial conformational change. This change is coupled to mechanistically critical rearrangements in the membrane-spanning domains associated with unidirectional substrate translocation, which is believed to occur through a tailored pathway at the domain interface. After the substrate has crossed the membrane, the transporter returns to the resting state through the dissociation of ADP and inorganic phosphate. As with other ATPases, orthovanadate inhibits ABC transporter function (*15*); for example, the bacterial maltose importer (MalFGM) was shown to be trapped close to the transition state, with ADP, ortho-vanadate, and the binding protein firmly associated, while the substrate (maltose) was already released (*16*). This suggests that during translocation, the maltose-binding protein may serve as a plug that prevents the substrate from escaping on the wrong side of the membrane. Similar experiments with the bacterial, drug-exporting LmrA

Howard Hughes Medical Institute and Division of Chemistry and Chemical Engineering, Mail Code 147-75CH, California Institute of Technology, Pasadena, CA 91125, USA.

*To whom correspondence should be addressed. E-mail: locher@caltech.edu, dcrees@caltech.edu

transporter revealed that the protein exposes substrate-binding sites with different affinities and on different sides of the membrane during the transport reaction (*17*).

In addition to the immense amount of biochemical data, advances have also been reported in visualizing ABC transporters; the structures of several ABC cassettes have been crystallographically determined and exhibit a similar core and ATP-binding site (*13*, *18*–*22*). Some of these structures were found to be monomeric; however, HisP, MalK, and Rad50 (a DNA repair enzyme homologous to ABC cassettes) were reported to be dimers, although with distinct arrangements in each case. The membrane-spanning domain of ABC transporters is generally believed to consist of a total of 12 transmembrane helices, although deviations from this number have been predicted for several transporters. The recently published structure of the *E. coli* lipid flippase MsbA at 4.5 Å resolution did indeed show a total of 12 transmembrane helices per dimer (*23*). The subunit arrangement observed in MsbA placed the two ABC cassettes some 50 Å apart from each other, with the projected ATP-binding sites, which were disordered in the crystal, facing away from the dimer center. Electron microscopy has also been used to investigate ABC transporters such as MDR1 and MRP1 (*24*, *25*). These studies were performed in lipid membranes and are therefore likely to capture the physiologically relevant assembly of an ABC transporter. However, the resolution was not sufficient to reveal the details of the domain arrangement.

Despite these advances in the characterization of ABC transporters, answers to mechanistically important questions have remained elusive: (i) How do the ABC cassettes interact in a fully assembled ABC transporter? (ii) What does the substrate translocation pathway through an ABC transporter look like? (iii) What conformational changes are involved in coupling ATP hydrolysis to transport across the membrane? To address these questions, we have determined the crystal structure of an ABC transporter, the *E. coli* vitamin B_{12} importer BtuCD, at 3.2 Å resolution, with all critical parts ordered and resolved.

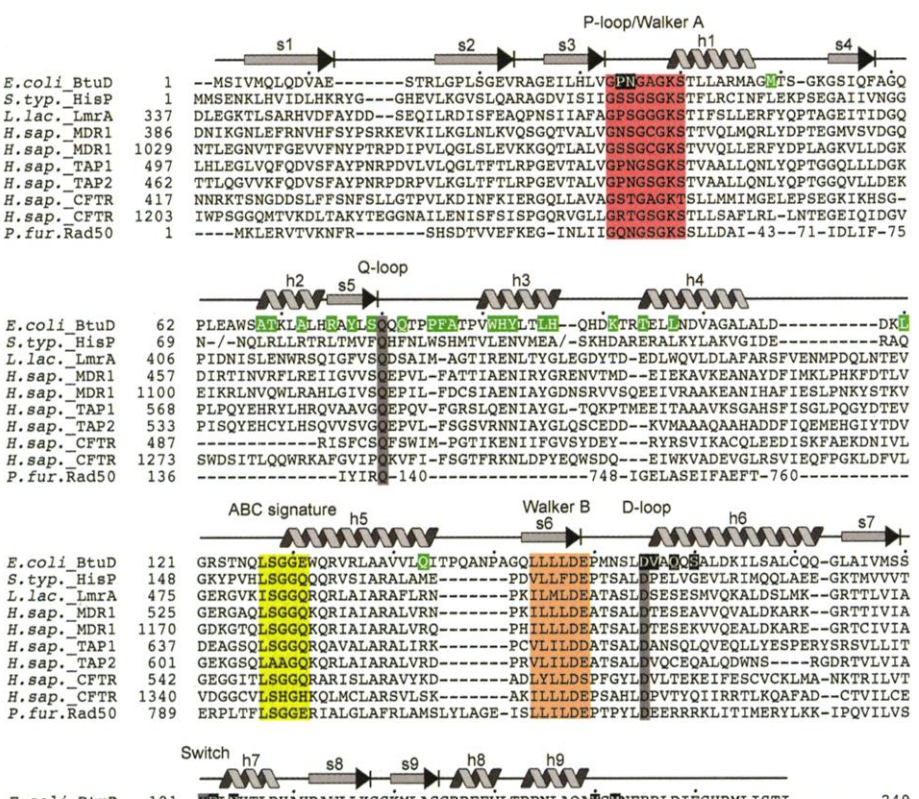

Fig. 1. Sequence alignment of the ABC cassette subunit BtuD with that of other transporters. Critical conserved motifs are indicated, with the corresponding residues designated by colored backgrounds (*57*). Secondary structure elements derived from the structure are indicated above the sequence. Residues involved in side-chain contacts (4 Å distance cutoff) between the ABC cassettes are shown in white on black background; those involved in side-chain contacts with the membrane-spanning BtuC subunit are white on green background.

Structure determination of BtuCD. Structure determination of ABC transporters has been experimentally challenging because of their dynamic nature in detergent solution, which very often inhibits formation of well-ordered, three-dimensional crystals. To optimize the likelihood of success, we subcloned the genes for 28 distinct ABC transporters originating from different biological sources and transporting diverse substrates, then tested their expression in *E. coli*. The set included both exporters and importers, with several composed of multiple subunits that were all coexpressed from a single plasmid. We varied the location of the poly-histidine tag (amino- versus carboxy-terminal) in all combinations for each subunit because of the known influence of the location of the tag on expression levels. A similar strategy was implemented in the structure determination of the *E. coli* mechanosensitive channel MscL (*26*).

Our screening approach yielded pure and stable preparations for several transporter-detergent combinations, which were all submitted to a large screening matrix for crystallization conditions (*27*). The best crystals were obtained for the *E. coli* BtuCD protein that mediates vitamin B_{12} uptake (*28*, *29*). Crystals diffracted anisotropically to beyond 3.2 Å resolution, with the diffraction data characterized by an extremely sharp falloff in intensity, corresponding to a Wilson-B factor of ~100 Å^2. Initial phases were obtained from two separate derivatives, which yielded the envelope of the molecule and the location of several of the transmembrane helices. These phases were used to locate, in two rounds, 34 selenium sites per full transporter in a selenomethionine three-wavelength anomalous diffraction data set (Table 1). The obtained phases yielded electron density maps at 3.5 Å resolution of excellent quality, and models of both the membrane-spanning subunits and the ABC cassettes could be built into the density. Helpful landmarks for model building were provided by the 34 selenium sites, seven gold sites indicating cysteines, and the position of two cyclotetravanadates bound to the P loop (Fig. 2A). With the exception of seventeen carboxyterminal residues of the BtuD subunit and a few amino acids in periplasmic loops of the membrane-spanning BtuC subunit, clear density was visible for the entire protein (Fig. 2B). A single model was used to refine the structure with bound cyclotetravanadate at 3.2 Å resolution, and details are given in Table 1.

Assembly of the BtuCD complex. The functional unit of the vitamin B_{12} transporter consists of two copies each of the BtuC and BtuD subunits and also corresponds to the crystallographic asymmetry unit. The transporter exhibits a molecular and noncrystallographic two-fold rotation axis, and the four

subunits assemble such that the two ABC cassettes are in close contact with each other, as are the membrane-spanning transport subunits. With the exception of the first periplasmic loop of BtuC that forms a lattice contact, the noncrystallographically related subunits of both BtuC and BtuD appear indistinguishable at the current resolution. The assembled complex is ~90 Å tall, ~60 Å wide, and ~30 Å thick, and when viewed from the front face (as presented in Fig. 3A), its overall shape resembles that of an inverted portal. At the center of the heterotetramer, below the predicted membrane surface and therefore exposed to the cytoplasm, a giant, water-filled channel crosses the flat face of the transporter (Figs. 2B and 3A). As a consequence, each subunit only contacts its two immediate neighbors and has no interface with the remaining, diagonally positioned subunit. This arrangement differs significantly from that observed for the lipid flippase MsbA, where the two ABC cassettes are separated by ~50 Å and the interface between the transmembrane subunits is limited to residues located near the periplasmic region. The BtuCD structure does not contain a region analogous to the intracellular (IC) domain present in MsbA, and therefore the ABC cassette BtuD is located just below the membrane surface. When viewed along the two-fold molecular axis, the long axis of the pair of ABC cassettes is rotated with respect to the long axis of the pair of membrane-integral BtuC subunits by approximately 25° (Fig. 3, B and C).

Structure and interface of the two ABC cassettes. The ABC cassette BtuD exhibits a similar polypeptide fold to that previously observed in the structures of HisP, MalK, TAP1, MJ1267, MJ0796, and the DNA repair enzyme Rad50 (*13*, *18*–*22*). The core consists of a six-stranded β-sheet that is surrounded by nine α-helices and a peripheral, three-stranded β-sheet. The structural similarity of these proteins is illustrated by the root mean square deviations in C_α positions between BtuD and other ABC cassettes of 1.86 Å for HisP (195 atoms), 1.50 Å for MalK (123 atoms), 1.92 Å for TAP1 (193 atoms), 1.90 Å for MJ1267 (162 atoms), 1.85 Å for MJ0796 (159 atoms), and 2.16 Å for Rad50 with bound ATP (164 atoms).

The interaction of ABC cassettes with each other in the active form of ABC transporters has been anticipated by a large body of biochemical evidence that has demonstrated strong cooperativity in ATP binding and hydrolysis (*12*). However, the exact arrangement and location of the contact interface between these cassettes have been controversial. Distinct dimeric arrangements have been proposed on the basis of the structures of the ABC cassettes of the bacterial histidine and maltose importers, HisP and MalK, and for the DNA repair enzyme Rad50 (*13*, *18*, *19*). Although it could not be excluded that different ABC transporters might possess distinct cassette arrangements, the Rad50 dimer has been predicted to represent the physiologically relevant one (*22*). The dimeric arrangement of the ABC cassettes in the present structure of the BtuCD transporter indeed resembles that found in the Rad50 dimer. The BtuD subunits are aligned side by side in a way that juxtaposes the ABC signature motif of one subunit to the P loop of the other. This arrangement places the likely nucleotide-binding site between the two opposing BtuD subunits. The dimer interface consists mainly of amino acid residues from two highly conserved sequence motifs, the P loop and the D loop, and from the moderately conserved Switch region, suggesting that this dimer arrangement may be common to all members of the family. Figure 1 indicates all the residues that are involved in side-chain contacts at the BtuD subunit interface. The two ABC cassettes bury only 740 $Å^2$ between them, which is rather small for a specific dimer contact surface and substantially smaller than the buried interfaces between each pair of BtuC-BtuD subunits or between the two BtuC subunits (see below). If the arrangement found for BtuCD is shared by all ABC transporters, the small contact surface between ABC cassettes may explain the formation of nonphysiological dimers of HisP and MalK in the absence of their membrane-integral partner subunits. In the case of Rad50, which lacks a partner protein, the stability of the dimer with bound ATP is maintained through a larger subunit interface than that between BtuD cassettes (*13*).

The nucleotide-binding site of BtuD closely resembles that of other ABC cassettes. All residues critical for ATP binding are conserved and present in the same locations. These include residues in the P loop, the two negatively charged residues from the Walker-B motif, a glutamine from the Q loop, and the histidine from the switch region (*11*). A vanadate species, introduced as a heavy atom derivative and identified as cyclotetravanadate, was found in the nucleotide-binding site of the BtuCD transporter. (Fig. 3, A and C). Cyclotetravanadate is the predominant species in aqueous solutions of ortho-vanadate at the pH used for growing BtuCD crystals (*30*), yet mono-vanadate is the form that inhibits ABC transporters. Examination of electron density maps calculated with diffraction data from vanadate-free crystals demonstrated that the presence of the cyclotetravanadate molecule did not perturb the structure of the ABC cassette subunit. When superimposed onto the ATP-binding site of HisP, Rad50, TAP1, MJ1267, and MJ0796 (all of which were solved with bound nucleotide), two of the vanadates closely superimpose with the α- and β-phosphates of bound nucleotide (Fig. 6).

Structure of the membrane-spanning BtuC subunit. Each of the two BtuC subunits traverses the membrane 10 times for a total of 20 transmembrane (TM) helices in the transporter (Fig. 3B). This number of

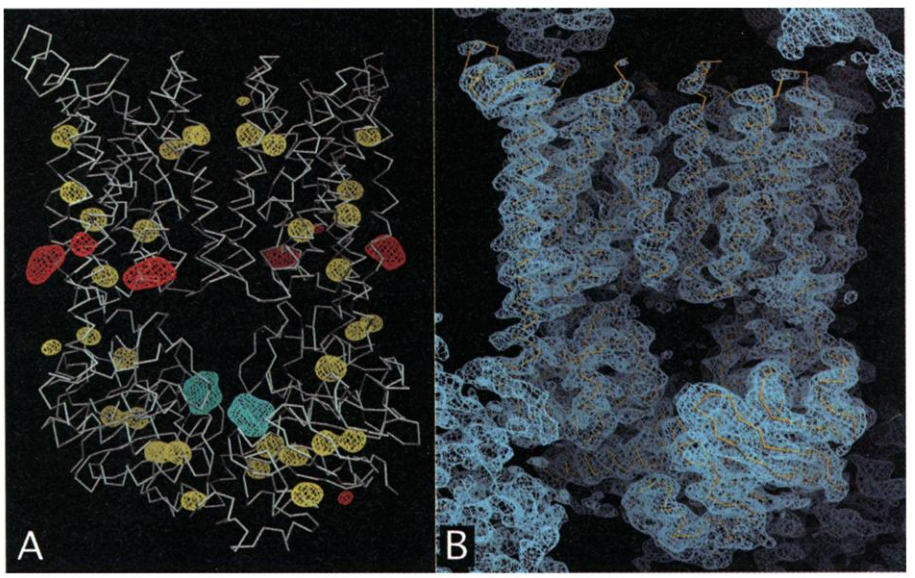

Fig. 2. Experimental electron density maps. (**A**) Side view of the backbone of a complete vitamin B_{12} transporter, with superimposed anomalous Fourier maps calculated from the selenomethionine (yellow, 3.5 Å resolution), gold (red, 4.5 Å resolution), and vanadate (cyan, 3.2 Å resolution) data sets. For clarity, the last is shown only in the vicinity of the bound vanadate species, but peaks also appear in this map for all ordered methionines and cysteines. All maps are contoured at 4σ. (**B**) Experimental density at 3.5 Å resolution from the selenomethionine data set, contoured at 1σ. The BtuCD backbone is shown in yellow, from the same view as in (A). The large gap between the subunits is visible at the center of the molecule, with lattice contacts evident in the corners of the panel. Figures 2 to 6 were prepared with DINO (*58*).

helices is substantially more than the 12 transmembrane helices that have been predicted for a canonical ABC transporter and have been observed in the MsbA structure (*23*). However, for the ferrichrome-transporting FhuB protein, 20 transmembrane helices were predicted on the basis of extensive topological studies (*31*), and more recent models of the human antigen transporter TAP also predict up to 19 helices (*32*). The variability in the number of transmembrane passes may reflect diverse architectures of the membrane-spanning domains, where the sequence similarities are generally low between different transporters, or the need for more transmembrane passes to translocate larger substrates such as vitamin B_{12}. Alternatively, difficulties in predicting transmembrane passes may have led to an underestimation of their number for other ABC transporters.

The 10 transmembrane helices found per BtuC subunit are packed together in a rather intricate way that does not resemble the arrangement of the six helices in an MsbA monomer (*23*). The amino-terminus of BtuC is located farthest from the interface between BtuC subunits, and TM1 is oriented nearly perpendicular to the membrane plane. TM2 crosses the membrane at an angle of ~30° to the membrane normal and is wedged between several other helices, dividing the protein into front and back faces. TM3 starts with an extended motif before becoming a standard helix. TM4 and TM5 adopt regular α-helical conformations, while the turn between these two helices forms the gate at the center of the transporter (see Fig. 3B and text below). The long periplasmic loop between TM5 and TM6 is only partly ordered in our electron density, and may be important for binding the periplasmic binding protein of vitamin B_{12}, BtuF (*33*). This loop crosses over to the side farthest from the BtuC dimer interface, where TM6 is located. The prominent cytoplasmic loop between TM6 and TM7 folds into two short helices, termed L1 and L2, both of which make extensive contact with the ABC cassette (see below). TM7 does not cross the membrane all the way to the periplasmic side, but rather leads to an extended stretch packed between several other helices in the core of the protein. TM8 through TM10 are located on the same face of the membrane-spanning subunit, and the carboxy-terminus is positioned close to the BtuC dimer interface, approximately 25 Å from the NH_2-terminus of BtuC. A pseudo-two-fold rotation axis relates two groups of four consecutive transmembrane helices and their connecting loops within a single BtuC subunit; the first group comprises TM2 through TM5, the second, TM7 through TM10. The rotation axis lies in the membrane plane and is oriented at an angle of ~20° with respect to the long axis of the BtuC dimer pair. The remaining two transmembrane helices, TM1 and TM6, are not related by this symmetry. Although the sequences of these related groups of transmembrane helices exhibit low similarity, their structural resemblance suggests that they represent basic building blocks in a modular assembly, which may also apply to other ABC transporters.

Interface between the two membrane-spanning subunits and translocation pathway. The interface between the two membrane-embedded subunits is formed by the

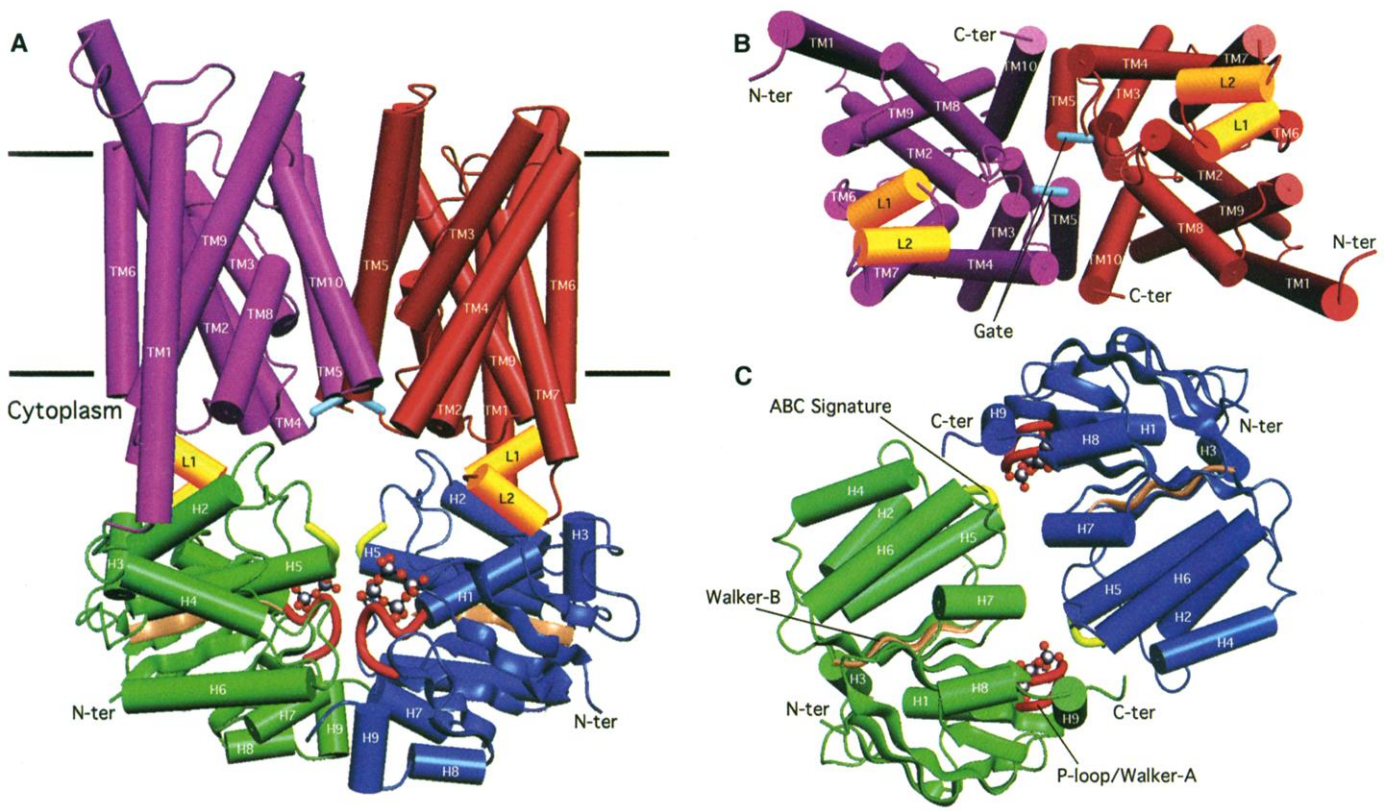

Fig. 3. Structure of the vitamin B_{12} transporter. The complete transporter is assembled from four subunits, two membrane-spanning BtuC subunits (purple and red), and two ABC cassette BtuD subunits (green and blue). Helices are drawn as cylinders and are labeled consecutively for each subunit, strands are shown as ribbons, and the amino- and carboxy-termini are labeled N-ter and C-ter, respectively. The cyclotetravanadate molecules, located in the ATP-binding sites, are depicted in ball-and-stick. The start and end residues of transmembrane (TM) helices in BtuC subunits are as follows: TM1 (2 to 32), TM2 (47 to 81), TM3 (93 to 107), TM4 (114 to 138), TM5 (142 to 166), TM6 (191 to 206), TM7 (229 to 249), TM8 (258 to 267), TM9 (272 to 296), TM10 (305 to 324). For corresponding residues of L1 and L2 refer to Fig. 5B. Functionally important motifs are labeled; for explanations, see text. (**A**) Side view of the full transporter, with the molecular and noncrystallographic two-fold rotation axis running vertically. Approximate boundaries of the membrane bilayer are indicated with horizontal lines, with the periplasmon at the top and the cytoplasm at the bottom. L1 and L2 denote helices in the cytoplasmic loop between the BtuC helices TM6 and TM7 (see text). (**B**) View onto the cytoplasmic face of the membrane-spanning BtuC subunits, along the molecular two-fold axis. (**C**) Bottom view onto the ABC cassette (BtuD) dimer from the same view as in (**B**). Note the ~25° angle between the long axes of the dimer pairs of BtuC and BtuD (see text).

antiparallel packing of TM5 of one subunit against TM10 of the other at a crossing angle of −143° and vice versa, with a total of ~1800 Å^2 buried surface. Between these four helices, a cavity is present that opens to the periplasmic space and spans two-thirds of the predicted lipid membrane. Although no substrate is present in our structure, this cavity is of sufficient size to accommodate much of a vitamin B_{12} molecule (Fig. 4) and likely represents the translocation pathway. The interior of the cavity is lined by hydrophobic residues provided by TM5 and TM10 and by the extended stretches preceding TM3 and TM8. The cavity is closed to the cytoplasm by residues Thr^{142} and Ser^{143} in the loops connecting TM4 and TM5 of each BtuC subunit. We refer to this region as the gate, as it separates the cavity at the BtuC dimer interface from the large gap at the center of the complete transporter (Fig. 3, A and B, and Fig. 4). Residues lining the periplasmic entrance to the presumed translocation pathway are only partly resolved in our structure (Fig. 2B), which likely reflects the absence of binding protein.

Contact region between the membrane-spanning BtuC and the ABC cassette BtuD. The cytoplasmic loop between the two transmembrane helices TM6 and TM7 of the BtuC subunit folds into two short helical stretches connected by a sharp bend. Both helices make extensive contacts with the ABC cassette BtuD. Because the shape resembles that of an L, with each arm formed by one of the helical stretches, we refer to this loop as the L loop, formed from helices L1 and L2. A total of ~1500 Å^2 surface area is buried between BtuC and BtuD, and although other parts of BtuC, such as the cytoplasmic loop between TM2 and TM3 and that between TM8 and TM9, as well as the cytoplasmic side of TM1, also contribute to the interface between the two subunits, the bulk is provided by L1 and L2 (Fig. 5A).

A comparison with the sequences of other ABC transporters reveals that the L loop may represent a general interface between ABC cassettes and membrane-spanning subunits/domains. There is local sequence similarity of this motif to the fourth intracellular loop of CFTR (ICL4), to the so-called "EAA loop" of bacterial importers (*34*), and to the first cytoplasmic loop in drug exporters (Fig. 5B). The functional relevance of this region has been demonstrated for CFTR, where several mutants in ICL4 influence gating, but not chloride conductance through the channel (*35*). Also, mutations in the corresponding regions of MalF and MalG, when present simultaneously, severely affect transport of maltose across the membrane (*34*). Furthermore, residues in the first cytoplasmic loop are critical for the function of human MDR1 (*36*). The corresponding region in MsbA has indeed

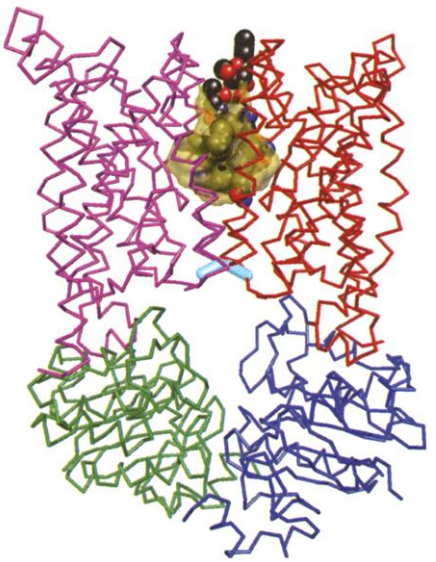

Fig. 4. Transport pathway for B_{12} through the BtuCD transporter. The backbone of the B_{12} transporter is shown in a side view, with the four subunits colored as in Fig. 3A. The cavity at the interface between the two membrane-spanning BtuC subunits is shown as a semi-transparent, yellow surface and was calculated with a probe radius of 2 Å using the program MSMS (*59*). The B_{12} molecule shown in CPK was manually docked into the cavity and is not present in the structure. The gate region is shown in light blue.

Table 1. Summary of structure determination. Crystals were in the space group $P2_1$ (a = 92.99 Å, b = 106.29 Å, c = 95.54 Å, β = 99.29°) with one complete transporter ($BtuC_2D_2$) per asymmetric unit. Data were processed with DENZO and SCALEPACK (*48*). For phasing, a combination of methods was applied using the programs XtalView (*49*), SOLVE (*50*), SHARP (*51*), and programs from the CCP4 suite (*52*). The locations of the vanadates were determined by inspection of the Patterson maps calculated at 5 Å resolution. Subsequently, several gold sites were located, and the phases were improved by combined solvent flattening and two-fold noncrystallographic averaging. The obtained phases were used to calculate anomalous cross-Fourier maps of data collected from a selenomethionine crystal at the peak wavelength. In two rounds, 34 selenium sites were located and their parameters refined. A model of the protein was built into the solvent-flattened and averaged maps using O (*53*). Refinement was carried out using CNS (*54*), and except for regions involved in lattice contacts, strict noncrystallographic symmetry was imposed. A model from the solved structure of cyclotetravanadate (*55*) was placed into the density, and its location was improved by rigid-body refinement. Group B factors were refined throughout, and the occupancy of side chains on the surface of the protein was set to zero if no density was visible. Model quality was verified with PROCHECK (*56*), and all residues are in the most favored or additionally allowed regions of the Ramachandran plot. MAD, multiple wavelength anomalous diffraction; rmsd, root mean square deviation.

Data set	Native	$Na_3Au(S_2O_3)_2$	o-vanadate	SeMet MAD			SeMet/o-vanadate
				Remote	Peak	Inflection	
Beam line	APS 19BM	APS 19ID	APS 19ID	SSRL 9-2	SSRL 9-2	SSRL 9-2	SSRL 9-2
Wavelength (Å)	0.9777	1.0394	0.9792	0.9184	0.9798	0.9800	1.7712
Resolution (Å)	30–4.0	50–4.0	50–4.0	30–3.5	30–3.5	30–3.7	30–3.2
Unique reflections	16265	15750	15828	23662	23433	19868	30660
Redundancy	4.5	8.2	7.6	4.5	7.5	3.7	8.2
Completeness*	98.3 (83.0)	98.6 (80.3)	99.3 (92.7)	99.5 (94.2)	99.1 (89.4)	99.0 (91.4)	99.5 (94.3)
$I/\sigma(I)$*	26.1 (8.3)	23.9 (8.3)	19.0 (10.5)	22.1 (6.8)	21.7 (7.6)	19.6 (9.0)	30.1 (4.1)
R_{sym} (%)*	4.4 (18.0)	7.5 (24.5)	9.5 (18.9)	6.1 (21.7)	8.1 (26.7)	5.7 (15.6)	6.7 (44.8)

Phasing from SeMet MAD data set		Refinement against SeMet/o-vanadate data	
Resolution (Å)	25–3.5	Resolution (Å)	15–3.2
Number of selenium sites	34	Reflections used	27122
Isomorphous phasing power from peak (centric/acentric)	2.75/4.14	Test reflections	2944
Anomalous phasing power from peak (acentric)	2.37	Number of nonhydrogen atoms†	7950
Isomorphous phasing power from inflection (centric/acentric)	2.33/3.66	R_{work} (%)	26.2
Anomalous phasing power from inflection (acentric)	1.96	R_{free} (%)	28.6
Figure of merit (centric/acentric)	0.53/0.65	Average B factor (Å^2)	101.6
		rmsd bond length (Å)	0.005
		rmsd bond angle (°)	1.12

*Numbers in parentheses refer to data in the highest resolution shell. †This number does not include atoms whose occupancy has been set zero.

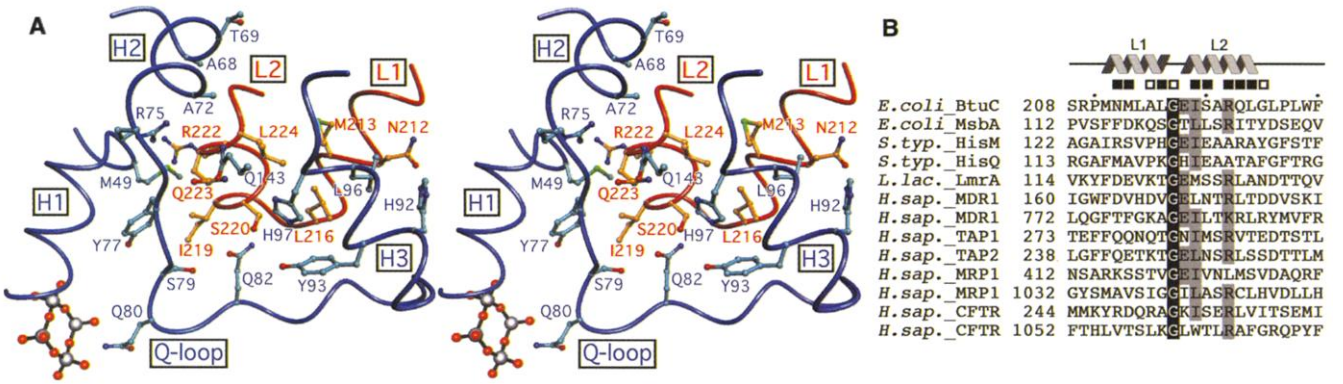

Fig. 5. Interface between the ABC cassette and the L loop of the membrane-spanning subunit. **(A)** The backbone of the contact regions of BtuD and BtuC are shown in blue and red, respectively. A distance cutoff of 4 Å was used to identify side chains contributing to the contact interface. Residues are depicted in ball-and-stick, with their numbers indicated in blue and red for BtuD and BtuC, respectively. The secondary structure elements are indicated by boxed labels. For a complete list of residues involved in the interface, see (B) and Fig. 1 (*57*). Gln^{80} and cyclotetravanadate in the lower left corner of the panel are shown to illustrate the proximity of the L-loop interface to the ATP-binding site. **(B)** Alignment of ABC transporter membrane domain/subunit sequences predicted to form the interface with their cognate ABC cassettes. The top row shows the vitamin B_{12} BtuC subunit, with secondary structure elements indicated above the sequence. Residues involved in side chain and backbone contacts with the ABC cassette BtuD are labeled with filled and open squares, respectively. Conserved residues have a light gray background in the area where sequence similarity is significant, and the well-conserved glycine is white on black background.

been found in contact with the ABC cassette in the recently published crystal structure (*23*). These observations support the functional significance of the L loop as a general interface between the ABC cassette and the membrane-spanning domain, and the moderate sequence similarity suggests that its structure may be common among ABC transporters, although the details of the interface with the ABC cassette may vary considerably. The finding that the L loop motif is present at different positions in the sequences of membrane-spanning domains of ABC transporters suggests that if such transporters possess a similar fold, they may exhibit circularly permutated connections in their respective membrane-spanning domains.

Residues around the Q loop dominate the surface of the ABC cassette BtuD involved in the interface with the membrane-embedded BtuC subunit (Fig. 1). Side chains making specific contacts to the L loop of BtuC are located in helices h2 and h3, and intervening regions, of BtuD (Fig. 5A). Two important exceptions are Met^{43} at the end of helix 1, which follows the P loop, and Gln^{143} in helix 5 after the ABC signature motif. In this way, elements involved in ATP-binding and hydrolysis may be coupled to the conformation of the L loop from the membrane-spanning subunit and vice versa. Mutations of residues involved in the interface with the L loop are expected to perturb the interface; a striking example is Leu^{96} of BtuD which corresponds to Phe^{508} in CFTR, whose deletion is the molecular basis of 70% of cystic fibrosis cases (*37*, *38*). Another example with clinical relevance is Gln^{143} of BtuD, which corresponds to Arg^{659} in TAP1. Mutation of this residue to a glutamine results in a 50% reduction of transport activity of the TAP protein when expressed in insect cells, and to a TAP-deficient phenotype of human lung cancer cells (*39*, *40*). Although the details in side-chain contacts may vary considerably, a comparable domain interface as the one observed between BtuC and BtuD can be expected between membrane-spanning domains and ABC cassettes of other ABC transporters, with proper assembly of that region being critical for coupling.

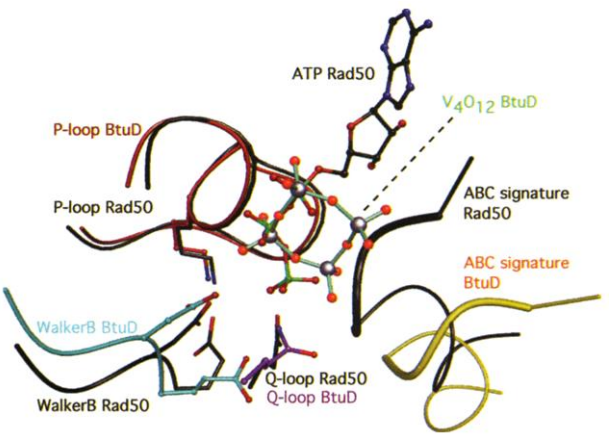

Fig. 6. Comparison of the ATP-binding sites of the ABC cassette dimers of BtuD and Rad50 (PDB entry 1F2U). Backbones and side chains of the two proteins are shown after superposition of the P loops. All structural elements belong to one ABC cassette, with the exception of the ABC signature sequence which belongs to the partner cassette in the dimer. Cyclotetravanadate and ATP are shown in ball-and-stick. Note the more distant locations of the ABC signature motifs in BtuD relative to Rad50 (see text for explanation).

Possible mechanism of vitamin B_{12} transport. During the transport cycle, ABC transporters undergo major conformational changes, as demonstrated by a number of biochemical assays and recently visualized at low resolution for the human MDR1 protein (*24*). The most significant rearrangement is believed to occur as the substrate is shuttled across the membrane and ATP is hydrolyzed. The present structure of BtuCD may be combined with previous biochemical and structural data to develop a plausible framework for the structural rearrangements associated with vitamin B_{12} transport.

In a first step, initiation of a productive transport cycle requires coupling of substrate binding to alterations in the nucleotide-binding site. In the case of exporters, the substrate and nucleotide-binding sites could be directly linked, because both are located on the cytoplasmic side of the membrane. In the case of importers such as the B_{12} transporter, the substrate and the nucleotide-binding sites are on opposite sites of the membrane and cannot be directly coupled. This implies that a signal must be transmitted from the periplasmic binding protein site across the membrane-spanning domain to the nucleotide-binding site; analogous signaling exists across the *E. coli* outer membrane after substrate binding to the ferrichrome transporter FhuA (*41*, *42*). Because the L loop provides the largest contribution to the BtuC-BtuD interface, it is well positioned for this signaling function.

In a second step, ATP hydrolysis is coupled to substrate translocation. It is evident from the present BtuCD structure that the membrane-

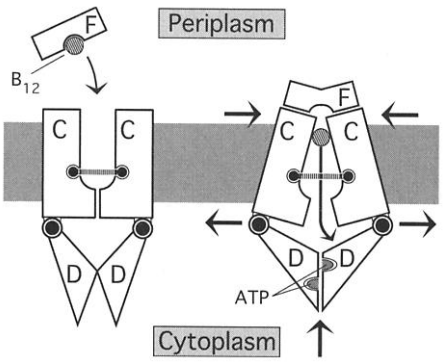

Fig. 7. Schematic mechanism of vitamin B_{12} import through the BtuCD transporter. The membrane-spanning and ABC cassette subunits are depicted as C and D, respectively, and the periplasmic binding protein BtuF as F. The gray ribbon represents the cytoplasmic membrane. On the left, the nucleotide-free state of the transporter is shown. On the right, proposed rearrangements during translocation of vitamin B_{12} are depicted. See text for further explanation.

spanning subunits, not the ABC cassettes, form the transporter gate, which is closed in the observed state (Fig. 3, A and B, and Fig. 4). This suggests that the role of the ABC cassettes is to control the conformation of the gate region through long-range conformational changes powered by binding and hydrolysis of ATP. Although it cannot be excluded that a cycle of association and dissociation of the ABC cassettes facilitate gate opening and closing (*13*, *23*, *43*), we favor a mechanistic model in which modulation of the existing interface between BtuD subunits triggers the conformational rearrangements that power substrate translocation. A hint at possible, nucleotide-dependent conformational changes in ABC transporters is provided by comparison of the BtuCD structure in the present, nucleotide-free state, to that of the DNA repair enzyme Rad50 in its dimeric, ATP-bound form (*13*). When both P loops of the BtuD subunits are superimposed onto those of the Rad50 dimer, significant, prominent differences are evident at the interface of the two ABC cassettes, where the ATP molecules are sandwiched between opposing subunits. In particular, the distance between the ABC signature motif and the P loop of opposing Rad50 subunits is ~4 Å shorter than that in the B_{12} importer. This likely reflects the presence of bound nucleotide, whose phosphates are wedged between the ABC signature and the P loop (Fig. 6). Furthermore, residues between the Walker-B motif and the D loop of each Rad50 cassette provide additional subunit contacts that are not observed in the BtuCD structure. Binding of ATP may induce a shortening of the distances between analogous regions of the B_{12} importer, resulting in a BtuD cassette interface similar to that observed in the Rad50 dimer. Such "closing" of the BtuD cassette interface with simultaneous narrowing of the subunit gap at both ATP-binding sites provides a plausible molecular explanation for the observed cooperativity in ATP binding in many ABC transporters.

In order to achieve such a rearrangement, the two BtuD cassettes may have to swing toward each other like the wings of a window shutter, because they appear firmly attached to the membrane-spanning BtuC subunits. In doing so, the two ABC cassettes could apply force directed from the cassette interface to the diametrically opposed contact regions with the L loops, which would consequently spread the membrane-spanning subunits and open the gate of the translocation pathway (Fig. 7). Such a mechanism would be analogous to the action of a toggle joint, a mechanical device that changes the direction of an applied force. The induced rearrangement of the two membrane-spanning BtuC subunits may be illustrated by the mechanism of a clothespin, where two moving arms are connected by a spring. The clamping function of the clothespin spring is meant to symbolize the extensive interface between the two membrane-spanning BtuC subunits, as well as the lateral pressure in the lipid bilayer, which together likely prevents a complete subunit dissociation during the transport cycle. Following the clothespin analogy, separation in the cytoplasmic halves of the BtuC subunits could thus be expected to narrow the periplasmic entrance of the translocation pathway. During such a rearrangement, the substrate would be released from the binding protein, cross the membrane through the provided pathway at the BtuC interface, pass the open gate, and exit through the large, water-filled gap at the center of the B_{12} transporter. The translocation may occur through diffusion, with the periplasmic entrance blocked by the binding protein, analogous to passage through an airlock. Alternatively, the substrate may be moved through the translocation pathway by peristaltic forces exerted by the membrane-spanning BtuC subunit. After the substrate has crossed the membrane, the transporter may return to its resting state through the release of ADP and inorganic phosphate, dissociation of the binding protein, closing of the gate, and reorientation of the ABC cassettes to their original position.

The mechanistic scheme depicted in Fig. 7, while reminiscent of the tilting model for ABC transporter function (*44*, *45*), differs from the scissors-type mechanism envisioned for lipid flipping by MsbA (*23*) in that both the ABC cassettes, as well as the transmembrane domains, remain in contact during the transport cycle. Because the subunits are treated as rigid entities, the proposed rearrangements may only represent part of the actual conformational changes, which are undoubtedly more complex. The mechanism presented here takes into account the presence of the ABC cassette dimer interface in the absence of bound ATP, the suggestive alignment of the ABC cassette dimer with the projected connection of the L loops (Fig. 3, B and C), and the presence of the large, water-filled gap between the ABC cassette interface and the membrane, likely representing the exit path of the substrate (Figs. 2B, 3A, 4). Alternative or additional motions during the transport cycle could involve a rotational component of the ABC cassettes or the membrane-spanning subunits, subdomain movements, or bending of membrane-spanning helices. In particular, rotational flexibility of the helical subdomain has been observed in several isolated ABC cassettes (*13*, *19*–*22*), but its relevance in fully assembled ABC transporters remains to be established. In this context, the significant structural differences of the Fe-protein in its free state or when attached to the MoFe-protein of nitrogenase are instructive (*46*): Although ATP is bound in both states, it is exclusively hydrolyzed by fully assembled nitrogenase. These observations highlight both the significance of structural information of complete ABC transporters, as well as its requirement for a detailed understanding of their transport mechanism.

Conclusions. The BtuCD structure provides a framework for the architecture of ABC transporters and a plausible mechanistic scheme for ATP-powered import of vitamin B_{12} into *E. coli*. The close contact between the BtuD subunits in the present, nucleotide-free conformation suggests that the power stroke in ABC transporters consists of a cooperative modulation of the ABC cassette interface upon ATP binding and hydrolysis, triggering rearrangements that control the conformation of the gate region between the membrane-spanning subunits and thus facilitating substrate permeation. The single translocation pathway at the interface of the membrane-spanning BtuC subunits is likely a common feature of ABC transporters of water-soluble substrates, although the size and the chemical nature of the internal surface may vary considerably. With 20 membrane-spanning helices, BtuCD has more transmembrane helices than the canonical prediction for ABC transporters. Although it cannot be excluded that this architecture is confined to importers involved in iron and B_{12} uptake [Fec-subclass of ABC transporters (*47*)], it may turn out to be more general. Alternatively, a common core structure of the membrane-spanning subunits may be present, with the surrounding helices varying among ABC transporters. The observed L loop as the prominent contact between the membrane-spanning subunit and the ABC cassette likely represents the lever transmitting the power stroke during ATP binding and hydrolysis, and appears to be present in membrane-spanning domains of all ABC transporters, although at different locations in their sequences. The present structure allows the re-evaluation of mutants of many ABC transporters, and suggests the design of further biochemical studies, including site-directed mutagenesis, that could probe the conformational

changes during the transport cycle. In addition, the BtuCD structure clears the way to structural studies of intermediate states, which should further advance our understanding of the translocation mechanisms.

References and Notes

1. See http://ir2lcb.cnrs-mrs.fr/ABCdb/.
2. S. C. Hyde *et al.*, *Nature* **346**, 362 (1990).
3. G. F. Ames *et al.*, *FEMS Microbiol. Rev.* **75**, 429 (1990).
4. D. N. Sheppard, M. J. Welsh, *Physiol. Rev.* **79**, S23 (1999).
5. M. M. Gottesman, S. V. Ambudkar, *J. Bioenerg. Biomembr.* **33**, 453 (2001).
6. R. Abele, R. Tampe, *Biochim. Biophys. Acta* **1461**, 405 (1999).
7. A. Kelly *et al.*, *Nature* **355**, 641 (1992).
8. W. Boos, J. M. Lucht, in Escherichia coli *and* Salmonella typhimurium: *Cellular and Molecular Biology*, F. C. Neidhardt *et al.*, Eds. (American Society for Microbiology, Washington, DC, 1996), vol. 1, pp. 1175–1209.
9. H. Nikaido, *Science* **264**, 382 (1994).
10. J. E. Walker *et al.*, *EMBO J.* **1**, 945 (1982).
11. E. Schneider, S. Hunke, *FEMS Microbiol. Rev.* **22**, 1 (1998).
12. I. B. Holland, M. A. Blight, *J. Mol. Biol.* **293**, 381 (1999).
13. K. P. Hopfner *et al.*, *Cell* **101**, 789 (2000).
14. F. A. Quiocho, P. S. Ledvina, *Mol. Microbiol.* **20**, 17 (1996).
15. I. L. Urbatsch *et al.*, *J. Biol. Chem.* **270**, 19383 (1995).
16. J. Chen *et al.*, *Proc. Natl. Acad. Sci. U.S.A.* **98**, 1525 (2001).
17. H. W. van Veen *et al.*, *EMBO J.* **19**, 2503 (2000).
18. L. W. Hung *et al.*, *Nature* **396**, 703 (1998).
19. K. Diederichs *et al.*, *EMBO J.* **19**, 5951 (2000).
20. R. Gaudet, D. C. Wiley, *EMBO J.* **20**, 4964 (2001).
21. N. Karpowich *et al.*, *Structure* **9**, 571 (2001).
22. Y. R. Yuan *et al.*, *J. Biol. Chem.* **276**, 32313 (2001).
23. G. Chang, C. B. Roth, *Science* **293**, 1793 (2001).
24. M. F. Rosenberg *et al.*, *EMBO J.* **20**, 5615 (2001).
25. M. F. Rosenberg *et al.*, *J. Biol. Chem.* **276**, 16076 (2001).
26. G. Chang, *Science* **282**, 2220 (1998).
27. Materials and methods are available as supporting material on *Science* Online at www.sciencemag.org/cgi/content/full/296/5570/1091/DC1.
28. P. R. Reynolds, G. P. Mottur, C. Bradbeer, *J. Biol. Chem.* **255**, 4313 (1980).
29. L. C. DeVeaux, R. J. Kadner, *J. Bacteriol.* **162**, 888 (1985).
30. E. Heath, O. W. Howarth, *J. Chem. Soc.-Dalton Trans.*, 1105 (1981).
31. W. Groeger, W. Koster, *Microbiology* **144**, 2759 (1998).
32. B. Lankat-Buttgereit, R. Tampe, *Physiol. Rev.* **82**, 187 (2002).
33. N. Cadieux *et al.*, *J. Bacteriol.* **184**, 706 (2002).
34. M. Mourez, N. Hofnung, E. Dassa, *EMBO J.* **16**, 3066 (1997).
35. J. F. Cotten *et al.*, *J. Biol. Chem.* **271**, 21279 (1996).
36. S. J. Currier *et al.*, *J. Biol. Chem.* **267**, 25153 (1992).
37. B. S. Kerem *et al.*, *Proc. Natl. Acad. Sci. U.S.A.* **87**, 8447 (1990).
38. L. C. Tsui, *Trends Genet.* **8**, 392 (1992).
39. H. L. Chen *et al.*, *Nature Genet.* **13**, 210 (1996).
40. L. Saveanu *et al.*, *J. Biol. Chem.* **276**, 22107 (2001).
41. K. P. Locher *et al.*, *Cell* **95**, 771 (1998).
42. A. D. Ferguson *et al.*, *Science* **282**, 2215 (1998).
43. P. J. Thomas, J. F. Hunt, *Nature Struct. Biol.* **8**, 920 (2001).
44. A. L. Davidson *et al.*, *Proc. Natl. Acad. Sci. U.S.A.* **89**, 2360 (1992).
45. C. F. Higgins, M. M. Gottesman, *Trends Biochem. Sci.* **17**, 18 (1992).
46. H. Schindelin *et al.*, *Nature* **387**, 370 (1997).
47. W. Koster, *Res. Microbiol.* **152**, 291 (2001).
48. Z. Otwinowski, W. Minor, *Methods Enzymol.* **276**, 307 (1997).
49. D. E. McRee, *J. Struct. Biol.* **125**, 156 (1999).
50. T. C. Terwilliger, J. Berendzen, *Acta Crystallogr.* **D55**, 849 (1999).
51. E. de la Fortelle, G. Bricogne, *Methods Enzymol.* **276**, 472 (1997).
52. CCP4, *Acta Crystallogr.* **D50**, 760 (1994).
53. T. A. Jones *et al.*, *Acta Crystallogr.* **A47**, 110 (1991).
54. A. T. Brünger *et al.*, *Acta Crystallogr. D Biol. Crystallogr.* **54**, 905 (1998).
55. M. T. Averbuchpouchot, A. Durif, *Eur. J. Solid State Inorg. Chem.* **31**, 567 (1994).
56. R. A. Laskowski *et al.*, *J. Appl. Crystallogr.* **26**, 283 (1993).
57. Single-letter abbreviations for the amino acid residues are as follows: A, Ala; C, Cys; D, Asp; E, Glu; F, Phe; G, Gly; H, His; I, Ile; K, Lys; L, Leu; M, Met; N, Asn; P, Pro; Q, Gln; R, Arg; S, Ser; T, Thr; V, Val; W, Trp; and Y, Tyr.
58. See www.dino3d.org.
59. M. F. Sanner *et al.*, *Biopolymers* **38**, 305 (1996).

60. We thank the staff at the Stanford Synchrotron Radiation Laboratory (SSRL), the Advanced Photon Source (APS), the Advanced Light Source (ALS), and the National Synchrotron Light Source (NSLS) for their support during crystal screening and data collection. We also thank M. Barclay, R. Bass, O. Einsle, I. Locher-Hinderling, and P. Strop for helpful discussions. We further thank M. Day for assistance in obtaining the cyclotetravanadate coordinates, and L. Ackerman and J. Bercaw for their help in the synthesis of inorganic clusters during the search for derivatives. The coordinates of the BtuCD transporter with bound cyclotetravanadate have been deposited in the Protein Data Bank (www.rcsb.org/pdb) with access code 1L7V.

21 February 2002; accepted 21 March 2002

REPORTS

Scanned Probe Imaging of Single-Electron Charge States in Nanotube Quantum Dots

Michael T. Woodside[1] and Paul L. McEuen[2]

An atomic force microscope was used to study single-electron motion in nanotube quantum dots. By applying a voltage to the microscope tip, the number of electrons occupying the quantum dot could be changed, causing Coulomb oscillations in the nanotube conductance. Spatial maps of these oscillations were used to locate individual dots and to study the electrostatic coupling between the dot and the tip. The electrostatic forces associated with single electrons hopping on and off the quantum dot were also measured. These forces changed the amplitude, frequency, and quality factor of the cantilever oscillation, demonstrating how single-electron motion can interact with a mechanical oscillator.

Single-electron charging phenomena are ubiquitous in atoms, molecules, and small electronic devices, and their effects are central to an understanding of the physics and technology of nanoscale systems. Single-electron effects arise because the number of electrons residing on a small, quasi-isolated, conducting island is quantized. Adding an additional charge to such a quantum dot costs an electrostatic energy on the order of $U = e^2/C$, where C is the capacitance of the dot and e is the electronic charge (*1*). This charging energy suppresses charge transport when $U \gg k_BT$, where k_BT is the thermal energy, leading to the Coulomb blockade of charge motion on and off the dot.

Although Coulomb blockade phenomena have been studied extensively with transport measurements (*2*), such measurements lack the spatial discrimination necessary to probe the interior of a dot or to probe complex multidot systems. An alternative approach is to detect single-charge motion using scanned probe techniques, such as scanned capacitance microscopy (*3*, *4*), scanned single-electron transistors (*5*, *6*), and atomic force microsopy (AFM). The first two of these have excellent charge sensitivity but are technically very difficult; moreover, they are not easily able to image the topography of the device under study. AFM-based techniques, on the other hand, can be used both to image the sample and to interact with it in a variety of ways. For example, electrostatic force microscopy (EFM), which measures the electrostatic force between a sample and a metallized AFM tip, has been used to detect the motion of single charges during contact electrification of insulating surfaces (*7*) and to image the potential profile in carbon nanotubes (*8*). In addition, scanned gate microsopy (SGM), in which the AFM tip is used to perturb the conducting properties of a sample, has been used to image electron trajectories and scattering centers in two-dimensional electron gases (*9*–*11*) and barriers in carbon nanotubes (*8*, *12*, *13*).

[1]Department of Physics, University of California, Berkeley, CA 94720, USA. [2]Laboratory of Atomic and Solid State Physics, Cornell University, Ithaca, NY 14853, USA.